

Role of Morphology and Förster Resonance Energy Transfer in Ternary Blend Organic Solar Cells

Aiswarya Abhisek Mohapatra, Ravichandran Shivanna, Suresh Podapangi, Alexander Hinderhofer, M. Ibrahim Dar, Nilabja Maity, Frank Schreiber, Aditya Sadhanala, Richard H. Friend,* and Satish Patil*



Cite This: *ACS Appl. Energy Mater.* 2020, 3, 12025–12036



Read Online

ACCESS |



Metrics & More



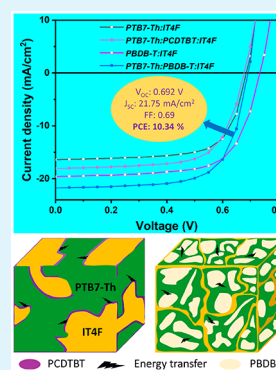
Article Recommendations



Supporting Information

ABSTRACT: Organic solar cells (OSCs) fabricated from ternary blend thin film absorbers are designed to maximize the range of absorption in the solar spectrum and thus increase the short-circuit current density (J_{SC}) of the device. Herein, we report OSCs formed with two different compositions of ternary blend thin films comprising two electron donors and one acceptor, namely, PTB7-Th/PCDTBT/IT4F and PTB7-Th/PBDB-T/IT4F. We evaluate the role of Förster resonance energy transfer (FRET) and blend morphology to achieve composition-dependent device performance. We observed $\geq 10\%$ increment in J_{SC} for both the ternary blends as compared to that for the PTB7-Th:IT4F binary blend, resulting in an enhanced power conversion efficiency (PCE) up to 10.34% for the PTB7-Th:PBDB-T:IT4F blend. We provide evidence that the two foremost parameters that control the PCE are blend morphology and FRET between donor components. The improved exciton generation rate for PCDTBT-based ternary blends was achieved, suggesting effective contribution of FRET toward enhanced device photocurrent, whereas the PBDB-T-based ternary blend excelled mainly due to suppressed carrier recombination as a result of favorable orientation with PTB7-Th/IT4F.

KEYWORDS: ternary blend organic solar cells, non-fullerene acceptor, Förster resonance energy transfer, blend morphology, suppressed carrier recombination, composition-tolerant device performance



1. INTRODUCTION

Organic solar cells (OSC) are one of the emerging photovoltaic technologies because they offer the prospect of semitransparency, solution processability, roll-to-roll production, and lightweight devices.^{1–3} Concerted efforts in design and synthesis of new donor materials, introduction of non-fullerene acceptors (NFA), and morphology control have led to a steady increase in the power conversion efficiencies (PCE) to more than 17%.^{4–9} NFAs, as replacement acceptors for fullerenes, are key to this efficiency improvement because of a wider absorption window in the solar spectrum, a greater degree of control over band gap, and better morphological properties.^{10–12} In the recent past, ternary blend organic solar cells (TBSCs) have been utilized to augment the light harvesting efficiency across the solar spectrum. The TBSCs are comprised of either two donors and one acceptor (D1/D2/A) or two acceptors and one donor (D/A1/A2) and have been able to deliver PCEs of $\sim 17\%$, which are higher than those of their respective best performing binary counterparts.^{13–16} The enhancement in PCEs of both binary and ternary blend solar cells is attributed to four important parameters: (i) increased open-circuit voltages (V_{OC}) by reducing the voltage loss due to nonradiative recombination to as low as 0.17–0.23 eV with newly developed NFAs,^{6,17–19} (ii) improved short-circuit current densities (J_{SC}) because of incorporation of NFAs with higher extinction coefficients extending to the near-

infrared (NIR) region (complementary to donor polymer absorption), which contribute substantially to the photocurrent generation in the wider spectral range,^{8,12,20} (iii) optimal offsets between the lowest unoccupied molecular orbitals (LUMO) of donor and acceptor moieties to simultaneously minimize the charge-transfer loss in V_{OC} and maximize the exciton dissociation,²¹ and last (iv) the charge extraction has been enhanced by the coordinated effect of choice of better hole/electron transport layers and superior interface engineering which has helped the fill factor (FF) reaching close to 80%.⁷ Nevertheless, the performances of these excitonic solar cells are far below the Shockley–Queisser limit, and there is full potential for improvement with the advent of novel D–A systems and minimizing the loss pathways.^{19,22,23}

Utilizing fundamental photophysical processes such as Förster resonance energy transfer (FRET) to harvest more excitons has been proved to be beneficial in many TBSCs.^{24–30} In addition, FRET has been effectively utilized to improve the

Received: September 6, 2020

Accepted: November 24, 2020

Published: December 7, 2020



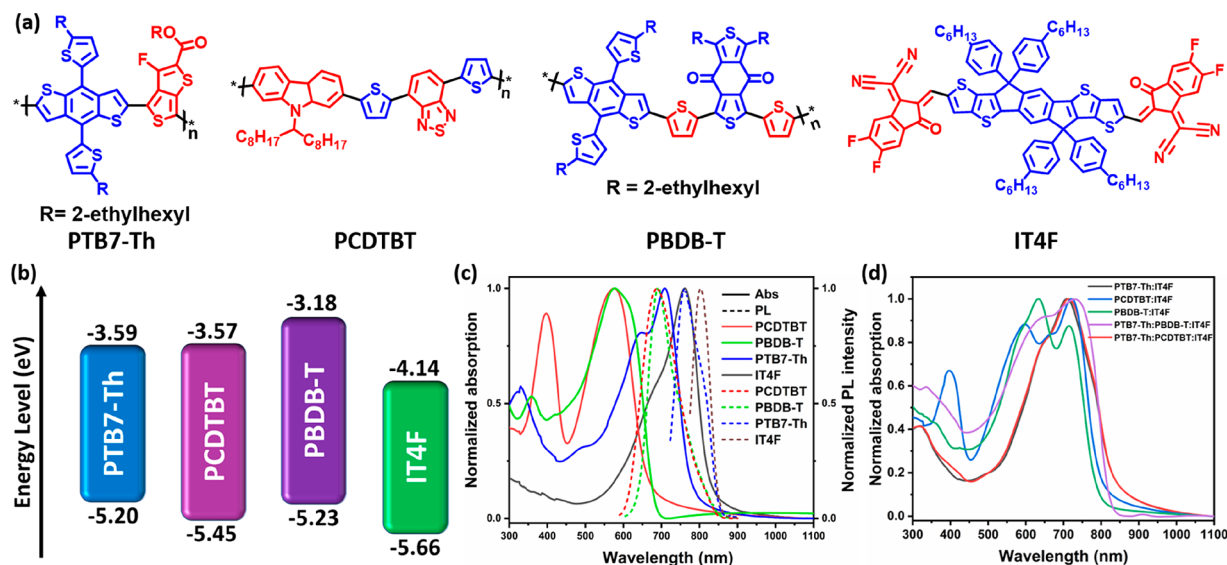


Figure 1. (a) Molecular structures of the three polymer donors, PTB7-Th, PCDTBT, and PBDB-T, and one small molecule acceptor, IT4F. (b) Energy level diagram of the four components showing alignment of frontier molecular orbitals with respect to the vacuum level to facilitate charge transfer upon light illumination. (c) Electronic absorption spectra of neat components (solid lines) and their corresponding PL spectra (dotted lines). The overlap of PL spectra of PCDTBT and PBDB-T with the absorption spectrum of PTB7-Th is evident. (d) Absorption spectra of the ternary blends showing extended spectral coverage until NIR by virtue of the non-fullerene acceptor IT4F. The weight ratio of PTB7-Th:PCDTBT:IT4F is 0.95:0.05:1, and that of PTB7-Th:PBDB-T:IT4F is 0.5:0.5:1.

device efficiencies by facilitating long-range exciton energy transfer in both multilayer and bulk heterojunction OPVs.^{31–33} FRET has been used effectively to minimize recombination losses both in active layer and in electron transport layer.^{34–36} In addition, the morphology of active layers can be tuned to have optimal nanoscale phase separation to facilitate exciton dissociation by addition of the third component which exhibits FRET with either D or A molecules.²⁹

In TBSCs, if the third component has a dominant charge transfer mechanism, then the V_{OC} is affected, whereas if it is an energy transfer mechanism, then the impact on V_{OC} is negligible.³⁷ In many TBSC systems, both the charge transfer and energy transfer (either Dexter or Förster type) processes coexist in a single blend which complicates the V_{OC} .³⁸ Depending on the nature of the third component, the active layer can adapt parallel-like or alloy-like models which have relaxed energy level constraints. In the parallel-like model, the third component serves as donor (or acceptor) and works independently with the existing donor (and/or acceptor). Then the ternary blend can be viewed as two subcells mixed together.³⁸ In the alloy-like model, the third component forms a homogeneous phase with one of the host components.³⁹ In this case, the other device parameters depend on physical miscibility and chemical compatibility of the two donors (or acceptors) in the ternary blend.²⁹

To probe and disentangle the role of blend morphology and resonance energy transfer, we investigated two ternary blend systems where two donor polymers, PCDTBT and PBDB-T, have been separately incorporated as third components in blends containing PTB7-Th as the primary donor and IT4F as the electron acceptor. We have established FRET between binary systems of PCDTBT:PTB7-Th and PBDB-T:PTB7-Th utilizing steady-state PL and transient absorption (TA) spectroscopy measurements. Both the ternary systems yielded higher PCEs than the control binary ones, and maximum PCEs of 8.28% for PTB7-Th:PCDTBT:IT4F and that of 10.34% for PTB7-Th:PBDB-T:IT4F were achieved. Although both the

polymers (PCDTBT and PBDB-T) exhibit FRET with PTB7-Th, we show the miscibility and phase morphology between them in the ternary blend play a decisive role in dictating their device performances. Both the binary and ternary blend OPVs were optimized by varying weight ratio of donor polymers, and we observed that only 5 wt % of PCDTBT with respect to PTB7-Th was sufficient to attain optimal morphology to deliver the highest PCE (8.28%), whereas incorporation of equal wt % of PBDB-T yielded 10.34% PCE. We further observed that the PBDB-T:PTB7-Th blends exhibited composition tolerance, resulting in ~10% PCE for various donor compositions because of better mixing of PBDB-T and PTB7-Th as reported previously.⁴⁰ The device characteristics were further analyzed to understand the origin of V_{OC} , exciton generation, dissociation, and charge collection probabilities in operating conditions. Composition-dependent V_{OC} was observed in both PCDTBT- and PBDB-T-based TBSCs due to formation of a homogeneous mixture. On the basis of atomic force microscopy (AFM), grazing incidence X-ray diffraction (GIXD) studies, and device characteristics, we propose that the PTB7-Th and PBDB-T form a parallel-like arrangement with IT4F, but PCDTBT forms an alloy with PTB7-Th in the respective optimized TBSCs. The contact angle measurements confirmed that PCDTBT is lying at the interface of PTB7-Th and IT4F, thereby facilitating the charge transfer at the interface. Suppressed bimolecular recombination in PBDB-T-based TBSC as compared to its binary counterparts resulted in increased photocurrent and consequently device efficiency. But the PCDTBT-based TBSC exhibited improved exciton generation, which is a cumulative effect of charge transfer, FRET between PCDTBT/PTB7-Th, and favorable blend morphology.

2. RESULTS AND DISCUSSION

2.1. Molecular Structure and Photophysical Properties.

The molecular structures of the four components, PTB7-

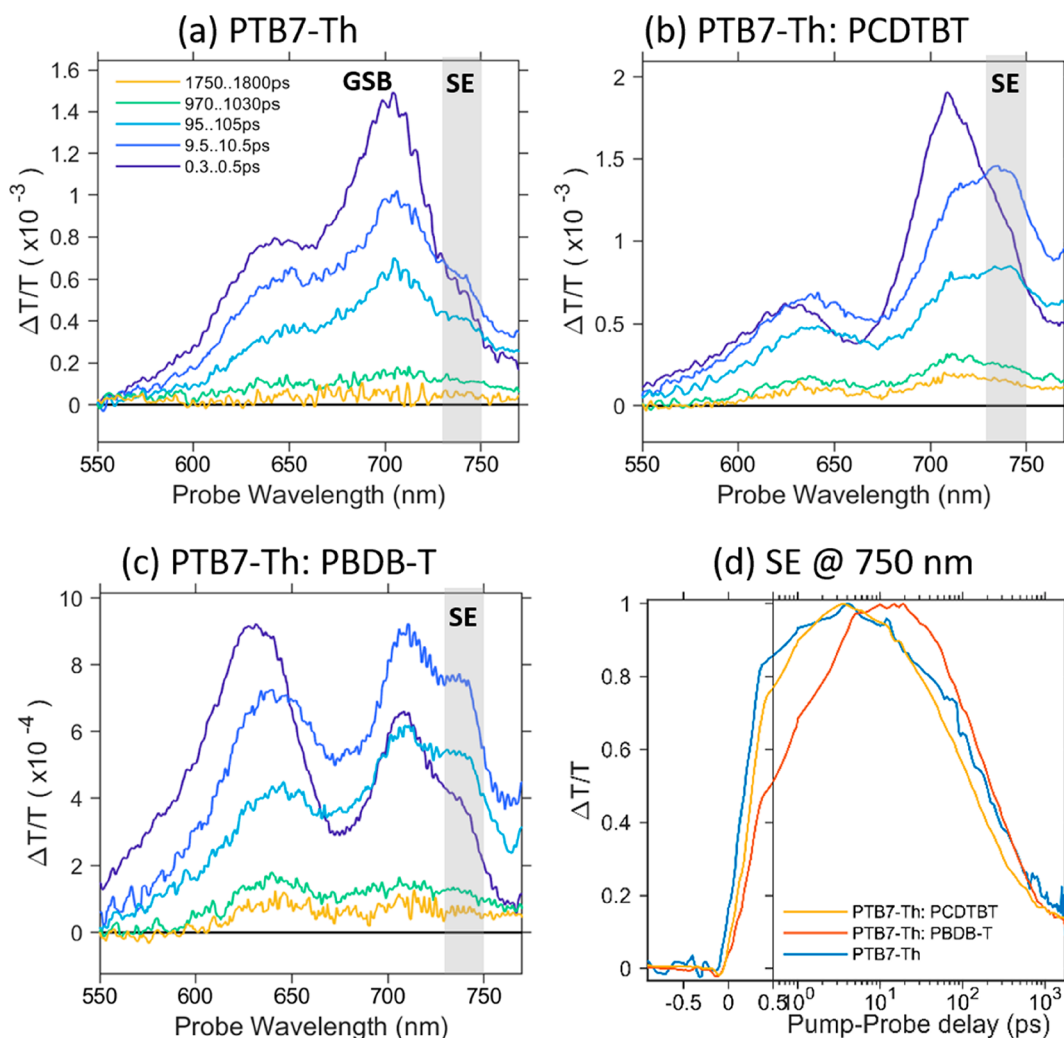


Figure 2. Transient absorption spectra at different intervals of time of (a) pristine PTB7-Th, (b) PTB7-Th:PCDTBT (50:50), and (c) PTB7-Th:PBDB-T (50:50). The films were pumped at 530 nm (FWHM ~ 10 nm, pulse width ~ 100 ns) with a fluence of $0.8 \mu\text{J}/\text{cm}^2$. The PTB7-Th exhibit GSB at 700 nm and SE at 750 nm. Both the blends show enhanced SE from the PTB7-Th, confirming the FRET between the polymers. (d) Normalized kinetics of SE from the PTB7-Th in logarithmic time axis (note the linear break at 0.5 ps). In blends, the SE exhibits a slower rise compared to pure PTB7-Th.

Th, PCDTBT, PBDB-T, and IT4F, utilized in two TBSCs are shown in Figure 1a. The donor–acceptor (D–A) type of structural arrangement in molecular backbones is a well-established strategy in organic semiconductor to facilitate intramolecular charge transfer and gain absorption in the near-IR range.^{6,8} The control binary system is PTB7-Th:IT4F, which forms a type II heterojunction for the efficient photoinduced charge generation process. The third component, either PCDTBT or PBDB-T, has a higher optical band gap and cascading energy levels with respect to PTB7-Th for the energy transfer process. In addition, PCDTBT has similar LUMO energy as that of PTB7-Th, facilitating the electron transfer process between PCDTBT, PTB7-Th, and IT4F, whereas PBDB-T has a similar highest occupied molecular orbital (HOMO) energy as that of PTB7-Th, facilitating the hole transfer process between PBDB-T, PTB7-Th, and IT4F (Figure 1b). The HOMO/LUMO levels of all the components were previously determined by utilizing cyclic voltammetry.^{12,41–43} Unidirectional electron transfer from PBDB-T to PTB7-Th because of a large LUMO offset and bidirectional hole transfer between PBDB-T/PTB7-Th has been reported in

the literature.⁴⁰ There have been reports on efficient hole/electron transfer with very low energy offsets without compromising charge carrier generation.^{21,40} Absorption spectra of the individual components along with the photoluminescence (PL) spectra of the polymer donors are shown in Figure 1c. Significant overlap of PL spectra of PCDTBT and PBDB-T with the absorption spectrum of PTB7-Th raises the possibility of FRET from either of the high band gap polymers to the lower band gap PTB7-Th.

Absorption spectra of the ternary blends with broader spectral coverage up to the NIR range are observed in both cases (Figure 1d). However, the contribution of PCDTBT towards the absorption of the best performing ternary blend is marginal considering the optimal loading percentage is only 5% with respect to PTB7-Th. Significant absorption of the PBDB-T based ternary blend in the visible part of the spectrum is because of equal weight percentages of PTB7-Th and PBDB-T in the optimal blend. The absorption spectra of binary and ternary blends are shown in Figure 1d; improvement in absorption at shorter wavelengths in both of the ternary blends upon introducing the third component is evident. To identify

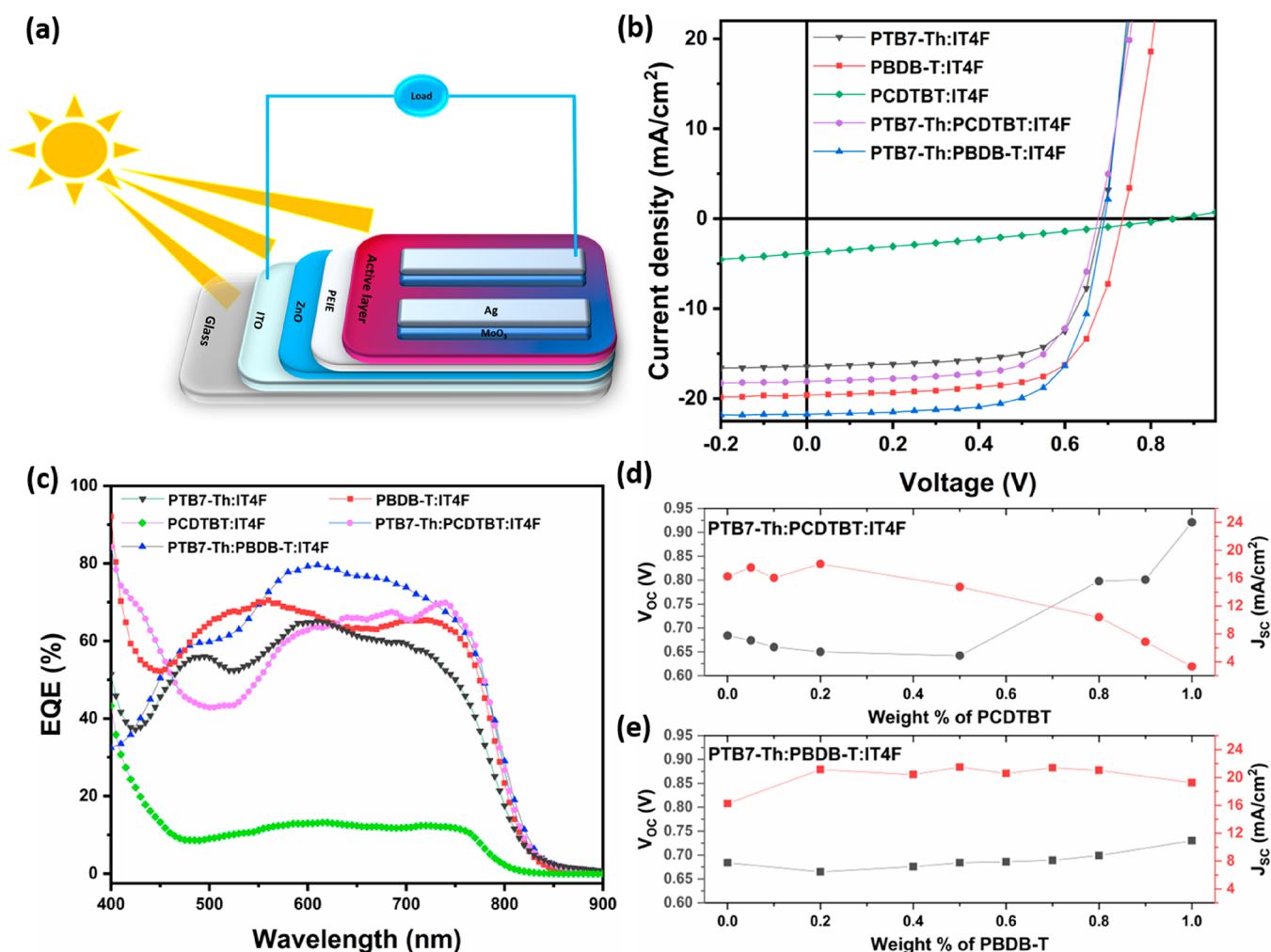


Figure 3. (a) Inverted solar cell architecture used for fabrication. (b) Current–voltage characteristics of binary and ternary blend photovoltaics showing highest current density for both the optimized ternary blends. (c) External quantum efficiency spectra of all the blends. Variation of V_{OC} and J_{SC} of (d) PTB7-Th:PCDTBT:IT4F (e) PTB7-Th:PBDB-T:IT4F cells, weight ratios of PCDTBT and PBDB-T with respect to PTB7-Th by keeping the combined donor to acceptor ratio of 1:1.

charge transfer from polymer donors to IT4F in binary and ternary blends, steady-state PL spectra of the blends were recorded by selectively exciting at 710 nm, corresponding to the absorption maximum of PTB7-Th. The quenching of PL of PTB7-Th is evident from Figure S1a with concomitant emergence of PL from IT4F at 805 nm. This shows efficient charge transfer from PTB7-Th to IT4F. The small hump near 805 nm corresponds to PL of IT4F which could be due to direct excitation of IT4F at 710 nm. Upon incorporation of 5% of the third component PCDTBT more than 97% of its PL was quenched, demonstrating photoinduced electron transfer between the three components as well as FRET between PCDTBT and PTB7-Th, which is verified from control experiments as discussed later. A similar trend was observed for the PBDB-T-based ternary blend system upon excitation at 520 nm (Figure S1a). A small hump near 805 nm can be observed in the PL from ternary blend which corresponds to emission from IT4F. The PL of PCDTBT and PBDB-T was effectively quenched upon addition of IT4F in equal quantity, suggesting effective photoinduced electron transfer and partial energy transfer because of overlap of emission spectra of PCDTBT/PBDB-T with the absorption spectrum of IT4F (Figure S1b). In summary, the PL quenching experiments

indicated the presence of both charge and energy transfer among the active layer components.

To establish FRET from PCDTBT to PTB7-Th independently, PL of the blends with varying ratio of PCDTBT and PTB7-Th was recorded by exciting the blend at 520 nm. A quantitative quenching of PL of PCDTBT was observed along with increase in sensitized emission from PTB7-Th (Figure S1c).⁴⁴ A similar trend was observed for PBDB-T:PTB7-Th blends (Figure S1d).⁴⁰ The PL quantum yield (PLQY) is another important parameter that gives an idea about charge/energy transfer between different chromophores.⁴⁵ Table S1 lists the quantum yields (QY) of neat polymers and binary blend films. To measure the PLQY of the neat and blend films, extra care was taken to prevent overestimation.⁴⁶ All the film thicknesses were kept similar (within a difference of 5 nm), and films were encapsulated to prevent any degradation. The slit bandwidths and excitation power of the laser were the same throughout. The increase in PLQYs of the blends with increased amounts of PCDTBT or PBDB-T indicates FRET between them. The FRET distances (R_0) between the polymeric pairs were calculated by using the dipolar approximation, the details of which are given in the Supporting

Table 1. Device Parameters of All the Optimized Blends Measured under 1 sun Illumination in Ambient Conditions Using an Intensity Calibrated AM1.5G Spectrum^a

active layers	V_{OC} (V)	J_{SC} (mA/cm ²)	FF (%)	PCE (%)	R_{sh} (k Ω -cm ²)	thickness (nm)
PTB7-Th:IT4F	0.685 (0.684 \pm 0.005)	16.42 (16.25 \pm 0.55)	69.70 (68.17 \pm 1.28)	7.84 (7.58 \pm 0.24)	0.77	71.7
PCDTBT:IT4F	0.855 (0.921 \pm 0.039)	3.81 (3.32 \pm 0.32)	28.66 (27.88 \pm 0.81)	0.93 (0.85 \pm 0.07)	0.26	107
PTB7-Th:PCDTBT:IT4F	0.677 (0.674 \pm 0.004)	18.08 (17.51 \pm 0.76)	67.64 (67.75 \pm 1.97)	8.28 (8.00 \pm 0.23)	0.69	66.9
PBDB-T:IT4F	0.734 (0.730 \pm 0.003)	19.60 (19.25 \pm 0.46)	67.85 (66.50 \pm 1.23)	9.76 (9.34 \pm 0.30)	0.84	75.6
PTB7-Th:PBDB-T:IT4F	0.692 (0.684 \pm 0.004)	21.75 (21.48 \pm 0.50)	68.73 (69.09 \pm 1.13)	10.34 (10.15 \pm 0.16)	9.15	93

^aThe weight ratios of all the binary blends are 1:1, PTB7-Th:PCDTBT:IT4F = 0.95:0.05:1, and PTB7-Th:PBDB-T:IT4F = 0.5:0.5:1.

Information. R_0 for PTB7-Th:PCDTBT was 4.1 nm, whereas that of PTB7-Th:PBDB-T was 3.1 nm.

To understand the FRET process, we utilized TA spectroscopy on these films. Probing spectral evolution of excited-state species at ultrafast time scales provides the dynamics of the energy and charge transfer processes. Here, we compared the TA data of pristine PTB7-Th and polymer blends PTB7-Th:PCDTBT and PTB7-Th:PBDB-T having 50:50 weight ratio. All the films are excited at 530 nm (FWHM \sim 10 nm, pulse width \sim 100 fs) by using an optical parametric amplifier (TOPAS) with a pump fluence of 0.8 μ J cm⁻². A low excitation density (below 1 μ J/cm² per pulse) is used to avoid annihilation processes of excited species and to simulate the solar cell operation conditions. The FRET acceptor, PTB7-Th, has a lower absorption coefficient (1/3 times) at 530 nm when compared to FRET donors PCDTBT and PBDB-T. Nonetheless, all the polymers can be excited by using a 530 nm pump. Figures 2a–c show the TA spectra in the range 550–770 nm at different intervals of time. In the pristine PTB7-Th, we observe positive bands at 700 and 640 nm, corresponding to ground-state bleach (GSB) consistent with the steady-state absorption (Figure 2a). Also, there is a positive shoulder arising at 750 nm corresponding to the stimulated emission (SE) of PTB7-Th. Similarly, the GSB and strong SE signals of pristine PCDTBT are observed at 580 and 700 nm, respectively (Figure S2a), whereas, for the pristine PBDB-T, the GSB is at 630 nm and the SE is masked by the photoinduced absorption (PIA) signal (Figure S2b). The strong SE signal in the PCDTBT compared to PBDB-T is consistent with the high PLQY of PCDTBT (Table S2). These features are retained in the 50:50 blends as shown in the Figures 2b,c. In the PTB7-Th:PCDTBT blend, the positive band at 700 nm (combined signal from GSB of PTB7-Th and SE of PCDTBT and vibronic band of PTB7-Th) is twice that of the 580 nm band (GSB of PCDTBT) from the early time (within 100 fs).

This is due to the fast energy transfer process for this blend (1.8 ps) and indicates that the PTB7-Th and PCDTBT are intermixed with domain sizes less than Förster radius. In the PTB7-Th:PBDB-T blend, the GSB of PBDB-T decreases with simultaneous increase in GSB of PTB7-Th up to tens of picoseconds. This suggests that the PTB7-Th and PBDB-T are phase-separated, and the rate of energy transfer is limited by exciton diffusion. The kinetics extracted from GSB arise from both radiative and nonradiative processes. Hence, to establish the FRET process unambiguously, we monitored the kinetics of SE of PTB7-Th (FRET-acceptor) at 750 nm in the blends. In both the films the SE feature of PTB7-Th is enhanced, confirming the FRET process at early times. Figure 2d represents the normalized kinetics of SE of PTB7-Th; note the x -axis is plotted in logarithmic scale with a linear break at 0.5 ps. Both the blends exhibit slow growth compared to pristine

PTB7-Th at a rate of 1.8 and 8.2 ps for PTB7-Th:PCDTBT and PTB7-Th:PBDB-T, respectively. This further confirms that both the blends are FRET active with different energy transfer rates due to different blend morphology. Following on, we calculated the efficiency of FRET using the equation⁴⁵

$$E_{\text{FRET}} = \frac{F_A}{F_A + F_D} \quad (1)$$

where, F_D and F_A are the PLQY of FRET donor and acceptor, respectively. The PLQY and E_{FRET} values for different neat materials and blends are tabulated in Table S1 of the Supporting Information. In both systems, increasing the donor ratio increases the E_{FRET} . The 50:50 blends of PTB7-Th:PCDTBT and PTB7-Th:PBDB-T exhibit E_{FRET} of \sim 27% and \sim 50%, respectively. E_{FRET} for the optimized blend ratio of 95:5 PTB7-Th:PCDTBT shows 14%, and for the 80:20 PTB7-Th:PBDB-T blend E_{FRET} is 33%. These results suggest that the polymers under study act as efficient FRET donor and acceptor systems, and in the subsequent section we will discuss the charge generation, transport, and collection of free charges in the TBSCs.

2.2. Device Characteristics. Both binary and ternary blend organic solar cells were fabricated in inverted architecture devices (Figure 3a). PTB7-Th:IT4F, PBDB-T:IT4F, and PCDTBT:IT4F cells were used as control devices to correlate with the performances of the ternary blends. The ternary blend comprised of PTB7-Th, PBDB-T, and IT4F delivered a highest PCE of 10.34% when blended in the 0.5:0.5:1 ratio by weight, respectively. PCDTBT when added in 5 wt % with respect to PTB7-Th delivered a maximum PCE of 8.28%. PBDB-T:IT4F yielded 9.76% PCE, which is on par with the reported values in the recent literature.⁴⁷ PTB7-Th:IT4F yielded 7.84% PCE, whereas PCDTBT:IT4F fared poorly because of poor morphology, which is discussed in later sections, and the resulting PCE was <1%. The average and best device parameters of all the blends, both binary and ternary, are tabulated in Table 1. PTB7-Th:IT4F and PBDB-T:IT4F interfaces were very efficient in charge generation, giving high current densities for both of them, whereas either of the PTB7-Th:PCDTBT/PBDB-T interfaces, by themselves, is unable to separate charge carriers as have been discussed in previously.^{44,48} From the J - V curves of all the blends in Figure 3b and Table 1, it can be seen that the J_{SC} of both the ternary blends are substantially higher than their best-performing binary counterparts. This can be attributed to the cumulative effect of improved sunlight absorption, resonance energy transfer, and balanced carrier extraction in ternary blends. The integrated J_{SC} values from EQE spectra (Figure 3c) were slightly less than the measured J_{SC} values within 7% errors, which may be due to the performance decay of the cells without encapsulation for EQE measurement. If the optimized

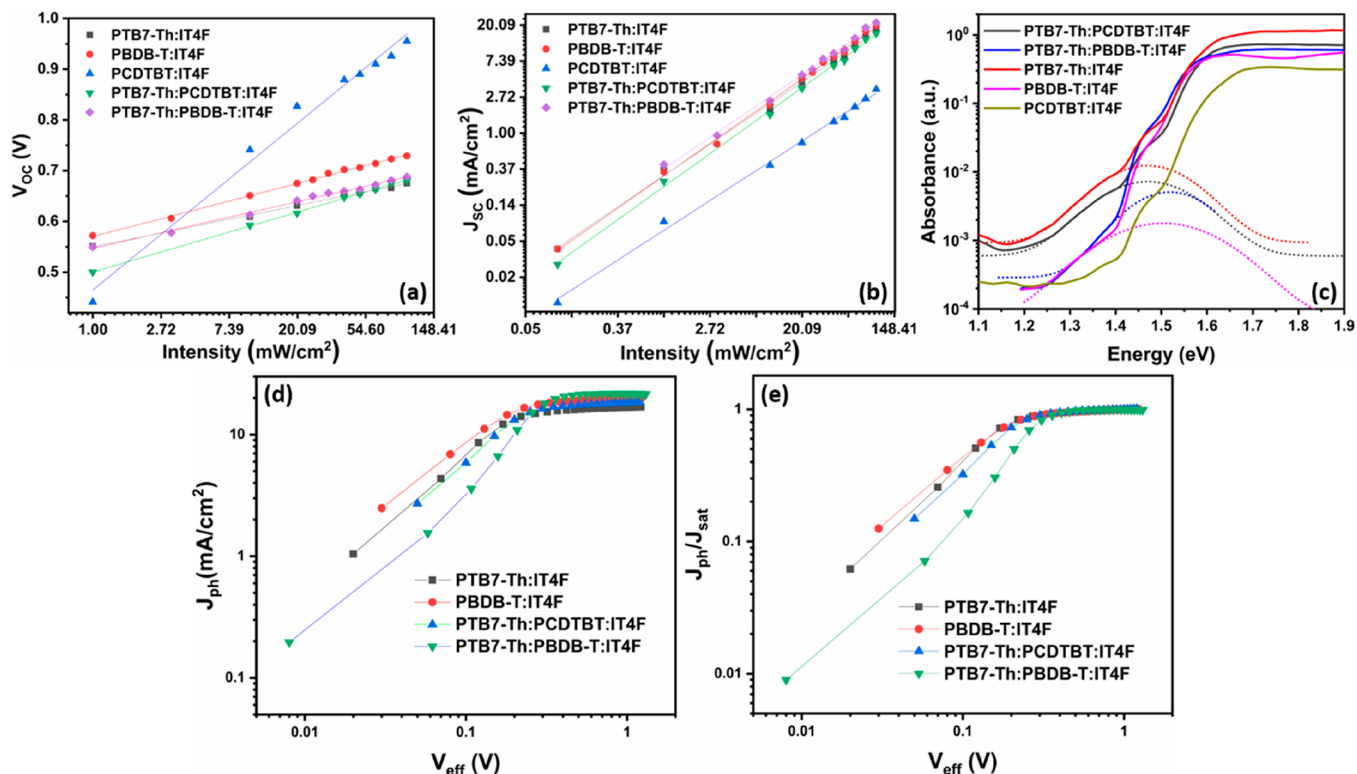


Figure 4. (a) Light intensity dependent (a) V_{OC} plot and (b) J_{SC} plot of all the optimized binary and ternary blend OPVs. (c) Photothermal deflection spectra of all the optimized blends; the dotted lines show Gaussian fitting to extract CT state energies. (d) V_{eff} vs J_{ph} of both binary and optimized ternary blends. (e) V_{eff} vs J_{ph}/J_{sat} of the same blends.

PTB7-Th:PCDTBT:IT4F (0.95:0.05:1) blend is considered, then the effect of improved absorption is less, considering that effectively 2.5 wt % of PCDTBT is in the blend, and the absorption spectra of ternary blend and that of binary blend (Figure 1d) show very little difference in the 500–600 nm range corresponding to PCDTBT absorption. FRET is present between PCDTBT:PTB7-Th, but considering the concentration of PCDTBT in the resulting blend, one would expect little contribution of FRET in boosting the current density.

The EQE of the ternary blend (Figure 3c) shows enhanced contribution from all the three components, emphasizing the contribution of a third component in generating photocurrent. Simultaneously, PCDTBT could be improving the charge extraction by balancing the charge mobility and enhancing the exciton dissociation by residing at the interface between PTB7-Th and IT4F, thereby suppressing bimolecular recombination. This is supported by the SCLC hole and electron mobilities as shown in Table S2. The J - V plots of all the optimized blends in hole-only and electron-only devices are shown in Figures S4 and S5. The higher carrier mobilities in the PCDTBT-based ternary blend mean reduced charge recombination and hence enhanced photocurrent. The shunt resistance (R_{sh}) of PTB7-Th:PCDTBT:IT4F is lower than that of PTB7-Th:IT4F, which could be the result of coarser film morphology as will be discussed in the following section. The improved R_{sh} for the PTB7-Th:PBDB-T:IT4F signifies lower leakage current and lower recombination as compared to the binary devices. In the case of PTB7-Th:PBDB-T:IT4F blend, the highest efficiency of the optimized blend with equal wt % PTB7-Th and PBDB-T is 10.34% with a J_{SC} of 21.75 mA/cm^2 . The improvement in J_{SC} can be attributed to improved spectral coverage, which is evident from EQE spectra in Figure 3c, and efficient FRET

between PTB7-Th and PBDB-T (1:1), which was established in the previous section. From the EQE spectra, the contribution from all the three components in improving the EQE toward 80% is very clear.

The device characteristics of TBSCs were investigated with varying donor compositions. The V_{OC} and J_{SC} of the ternary blends were plotted as a function of donor compositions in Figure 3d. It is observed that the V_{OC} and J_{SC} values of PTB7-Th:PCDTBT:IT4F ternary blend show a strong composition dependence as compared to PTB7-Th:PBDB-T:IT4F blends. In the case of PTB7-Th:PCDTBT:IT4F, V_{OC} decreases marginally upon increase in concentration of PCDTBT until the equal wt % of PCDTBT and PTB7-Th and rises at higher PCDTBT concentration as the device is controlled by the PCDTBT:IT4F heterojunction. The J_{SC} , largely dependent on successful charge extraction and favorable morphology, increases until 20% PCDTBT but then decreases rapidly as the concentration of PCDTBT became higher and higher. It was clear from the poor performance of PCDTBT:IT4F that PCDTBT does not yield compatible morphology with IT4F despite the favorable energetics, which is well evident from the AFM images shown in a later section. Hence, with only 5% PCDTBT, optimal performance was achieved. The blends with a higher amount of PCDTBT did not perform well although the FRET between PTB7-Th and PCDTBT becomes efficient with a higher amount of PCDTBT (Tables S1 and S3). This gives an important conclusion that FRET is necessary but not sufficient enough to boost the device performance because of the larger role played by blend morphology. However, the case of PTB7-Th:PBDB-T:IT4F was different because either of the donors is very compatible with IT4F and delivers higher PCEs. The V_{OC} of the optimal blend, i.e., that with 1:1 PTB7-

Th:PBDB-T, is 0.692 V. The HOMO levels of both PTB7-Th and PBDB-T have only a 30 meV offset, and a parallel-like arrangement of the two donors with IT4F is very much possible to pin the V_{OC} to the material with a higher HOMO level (here it is PTB7-Th).^{14,38} It is noteworthy to mention that the ternary blends consisting of varied percentages of PBDB-T performed well, and the J_{SC} values for all the ratios were above 20 mA/cm² (Table S4), suggesting that PTB7-Th and PBDB-T exhibit favorable morphology with the IT4F along with an additional energy transfer pathway between them.

2.3. Study of Charge Recombination. Light-intensity-dependent device characteristics give a qualitative picture about the operating recombination loss mechanisms in solar cells. At open circuit conditions, as all the photogenerated charge carriers are forced to recombine, V_{OC} as a function of intensity (I) provides an idea about the underlying recombination mechanisms (Figure 4a). The plot of V_{OC} vs $\ln(I)$ gives a slope equal to $n(k_B T/q)$, where n is the ideality factor of the diode. If n is close to unity, then the bimolecular recombination is the dominant loss mechanism at open circuit conditions. If n is close to two, monomolecular or Shockley–Read–Hall type recombination is dominant.⁴⁹ As can be seen from Table S5, the PTB7-Th:IT4F-based cell has n equal to 1.05, which means the majority of recombination loss is occurring through the bimolecular mechanism. The PCDTBT:IT4F blend has a very high n value of 4.24, indicating that the blend is suffering from traps or defects and trap-assisted monomolecular recombination is dominant. PBDB-T:IT4F has a n value of 1.35, which indicates that there might be monomolecular recombination along with dominant bimolecular recombination.^{49,50} In the ternary blend based on PCDTBT, the n value is around 1.52, suggesting the recombination mechanism is a mixture of monomolecular and bimolecular. In contrast, the PBDB-T-based ternary blend ($n = 1.18$) exhibits bimolecular recombination as dominant loss mechanism. The slope (α) of J_{SC} vs light intensity, both plotted in logarithmic scale, if close to unity, reflects about weak bimolecular recombination at short circuit and shows that all the generated carriers are swept out prior to recombination.^{51–53} The intensity vs J_{SC} plots for all the binary and ternary blends are shown in Figure 4b. If $\alpha < 1$, then it could be due to bimolecular recombination,⁵⁴ space charge effects,⁵⁴ variations in mobility between hole and electron, or variation in the continuous distribution in the density of states.⁵⁵ In our case as can be seen from Table S5 that all the binary and ternary blends have $\alpha < 1$, which can be attributed to the variation in electron and hole mobilities as inferred from the SCLC measurements (Table S2).

To understand more about the recombination mechanism in both the ternary blends, we plotted current–voltage characteristics of both the ternary blends for incident light intensities ranging from 1 to 100 mW/cm², as shown in Figure S6. The photogenerated current density ($J_{photo}(I, V)$) can be derived by subtracting the current density in the dark from the total current density flowing through the cell.⁵⁶ From Figures S6a and S6b, it is clear that the current density becomes independent of the applied voltage around -0.4 V (reverse bias). Therefore, the reverse saturation current can be assumed as $J_{photo}(V = -0.4 \text{ V})$, and the charge collection probability $P_C(I, V)$ can be given as

$$P_C(I, V) = \left| \frac{J_{photo}(I, V)}{J_{photo}(I, -0.4 \text{ V})} \right| \quad (2)$$

The charge collection probabilities of PTB7-Th:PCDTBT:IT4F and PTB7-Th:PBDB-T:IT4F are shown in Figure S7. The change in recombination kinetics with voltage, evolving from first order (monomolecular) in carrier density at short circuit to second order (bimolecular) near open circuit, was evident for PTB7-Th:PCDTBT:IT4F-based TBSC (Figure S7a). In contrast, bimolecular recombination was found to be a dominant loss mechanism for PTB7-Th:PBDB-T:IT4F-based TBSC as evident from Figure S7b. This was supported by the intensity-dependent studies of both the blends which showed n values in between 1 and 2 for PCDTBT-based TBSC and n values close to 1 for PBDB-T-based TBSC. Both the blends maintained high charge collection probabilities near the short circuit, which shows that these blends' internal quantum efficiencies (IQE) are very high.

2.4. Exciton Dissociation and Charge Collection. To understand more about the exciton dissociation and charge extraction processes, we plotted the photogenerated current density (J_{ph}) versus effective voltage (V_{eff}) for all the blends, where J_{ph} is defined as $J_{light} - J_{dark}$, and the $V_{eff} = V_0 - V$. J_{light} is the current density under illumination, J_{dark} is the current density in the dark, V_0 is the voltage at which $J_L = J_D$, and V is the applied external voltage (Figure 4d). The charge collection probability, $P(E, T)$, is defined as J_{ph}/J_{sat} , which is the same as $P_C(I, V)$ discussed in the previous section. The charge collection probabilities at short circuit as well as at maximum power point extracted by using this are tabulated in Table S5 for all the blends except PCDTBT:IT4F because of the ohmic nature of its J – V curve. The $P(E, T)$ values for ternary blends are within 1% of the previously calculated values. As compared to the binary blends, both the ternary blends have higher charge collection probabilities. As the exciton dissociation and charge extraction processes are closely related to $P(E, T)$, higher $P(E, T)$ values signify more efficient exciton dissociation and charge extraction processes.^{14,40,47} Upon introduction of PCDTBT or PBDB-T in the PTB7-Th:IT4F blend, the enhanced D/A interface suppressed geminate recombination and enhanced the free charge generation, thereby resulting in improved J_{SC} for both the ternary blends. At maximum power output point, the $P(E, T)$ for both the ternary blends were higher than their respective binary ones, which signifies that the charges are being collected efficiently upon dissociation (Figure 4e).⁵⁷ Another important parameter is the maximum exciton generation rate (G_{max}), which can be calculated via the equation

$$J_{sat} = eG_{max}L \quad (3)$$

where e is the electronic charge and L is the active layer thickness. The active layer thicknesses of all the optimized blends are shown in Table 1. From Table S4, the G_{max} of the PCDTBT-based ternary blend is higher than that of PTB7-Th:IT4F, but for the PBDB-T-based ternary blend, the G_{max} is $1.46 \times 10^{22} \text{ cm}^{-3} \text{ s}^{-1}$, which is the same as that of PTB7-Th:IT4F but lower than that of PBDB-T:IT4F. This could be due to the fact that the optimized thickness of the PTB7-Th:PBDB-T:IT4F blend was higher than that of PBDB-T:IT4F. Therefore, for the PBDB-T-based ternary blend, the exciton generation rate is comparable to that of the control

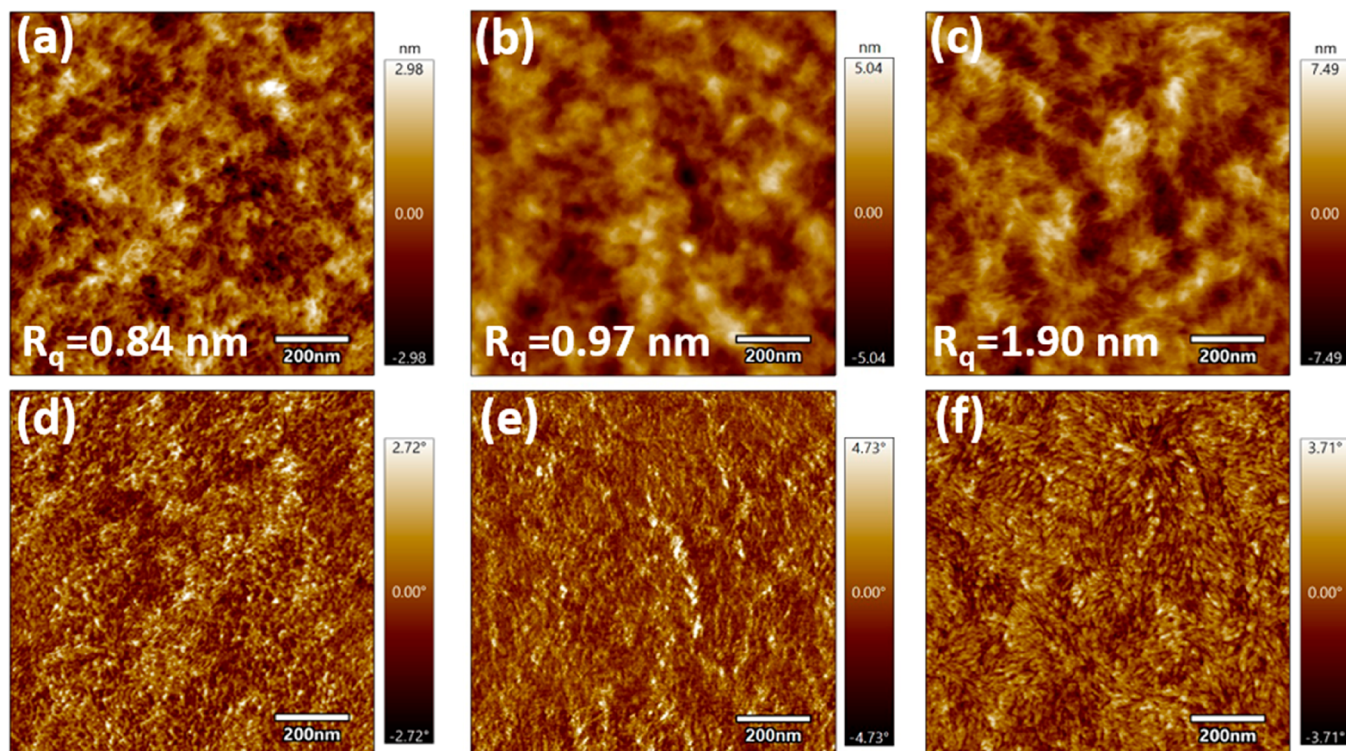


Figure 5. AFM height images of (a) PTB7-Th:IT4F (1:1), (b) PTB7-Th:PCDTBT:IT4F (0.95:0.05:1), and (c) PTB7-Th:PBDB-T:IT4F (0.5:0.5:1) (the RMS roughness values are shown as insets). The corresponding phase images are in the same order from (d) to (f).

binary ones. This signifies that the FRET does not play a prominent role in this case in generating more excitons, unlike the PCDTBT-based TBSC. Hence, the improvement in photocurrent in the case of PBDB-T-based TBSC can be attributed to lower recombination as suggested by the high value of R_{sh} (Table 1). The G_{max} of all the binary and TBSCs, except PCDTBT:IT4F, are comparable, signifying that the exciton generation rate is not compromised upon addition of third component; rather, it is marginally enhanced for the blend based on PCDTBT, which can be attributed to FRET and improved blend morphology as will be discussed later.

2.5. Charge Transfer State and Voltage Loss. The low oscillator strength of CT absorptions usually shows up as a hump in the lower energy tail of blend absorption spectra, and we measured it here using photothermal deflection spectroscopy (PDS) (Figure 4c). We performed Gaussian fitting to extract the energy of CT state maxima (E_{CT})⁵⁷ along with the reorganization energy (λ) involved (Figure 4c). The difference between E_{CT} and qV_{OC} is the energy loss resulting from both radiative and nonradiative recombination. Table S6 depicts the values of E_{CT} , λ , and energy loss of all the optimized binary and ternary blends along with the equation used for fitting the spectra. The photothermal deflection spectrum of PTB7-Th:IT4F resembles that of PTB7-Th:PCDTBT:IT4F (Figure S8a). Both the systems have similar λ and V_{OC} values; the E_{CT} and voltage losses are very similar, too. This implies that the introduction of low amounts of PCDTBT did not affect the interfacial CT state; instead, it formed an alloy with the primary donor PTB7-Th. Although the PDS of PBDB-T:IT4F resembles with that of PTB7-Th:PBDB-T:IT4F (Figure S8b), the introduction of PBDB-T lowered the reorganization energy of the resulting ternary blend and raised the E_{CT} to 1.38 eV. However, for PCDTBT:IT4F, the CT state could not be extracted from the PDS spectrum (Figure 4c).

2.6. Morphology Characterization. The blend morphology was characterized by using atomic force microscopy. The binary blend of PTB7-Th:IT4F shows a smoother surface with RMS roughness $R_q = 0.84$ nm (Figure 5a). When PCDTBT (2.5 wt % of total) is incorporated in the PTB7-Th:IT4F blend, the roughness of the resulting ternary blend increased marginally, and the phase image shows a high degree of miscibility between the components, which suggests that a little amount of PCDTBT could just be facilitating efficient charge transfer and energy transfer without disrupting the local morphology (Figure 5b,e). The height and phase images of the binary blends PCDTBT:IT4F and PBDB-T:IT4F are shown in Figure S9a,b,d,e. The PCDTBT:IT4F showed phase-separated domains which corroborates with its poor device performance, whereas PBDB-T:IT4F has high roughness as reported previously in the literature.⁴⁷ For the films having 25 wt % of PBDB-T (compared to total) incorporated in PTB7-Th:IT4F, both the height and phase images (Figure 5c,f) clearly show phase pure domains, although the surface RMS roughness doubled as that of PTB7-Th:IT4F. To see the effect of polymer weight percentage ratio, we recorded AFM height and phase images of PTB7-Th:PBDB-T:IT4F (0.8:0.2:1), and not surprisingly, the roughness of that was very similar to that of the 0.5:0.5:1 blend (Figure S9c). The phase image showed interpenetrating networks like the 0.5:0.5:1 blend which helped deliver more than 10% PCE (Figure S9f).

The blend crystallinity was characterized by using grazing incidence X-ray diffraction (GIXD) (Figure 6). Figure 6a shows data from the binary blend PBDB-T:IT4F exhibiting a pronounced out-of-plane stacking ($q_z = 3.14$ nm⁻¹). This corresponds to the stacking of pure PBDB-T.⁵⁸ Upon intermixing of PTB7-Th (Figure 6b–d), the out-of-plane stacking shifts to $q_z = 3.83$ nm⁻¹. We find that this is not a gradual shift, but instead, we find two distinct lattice spacings,

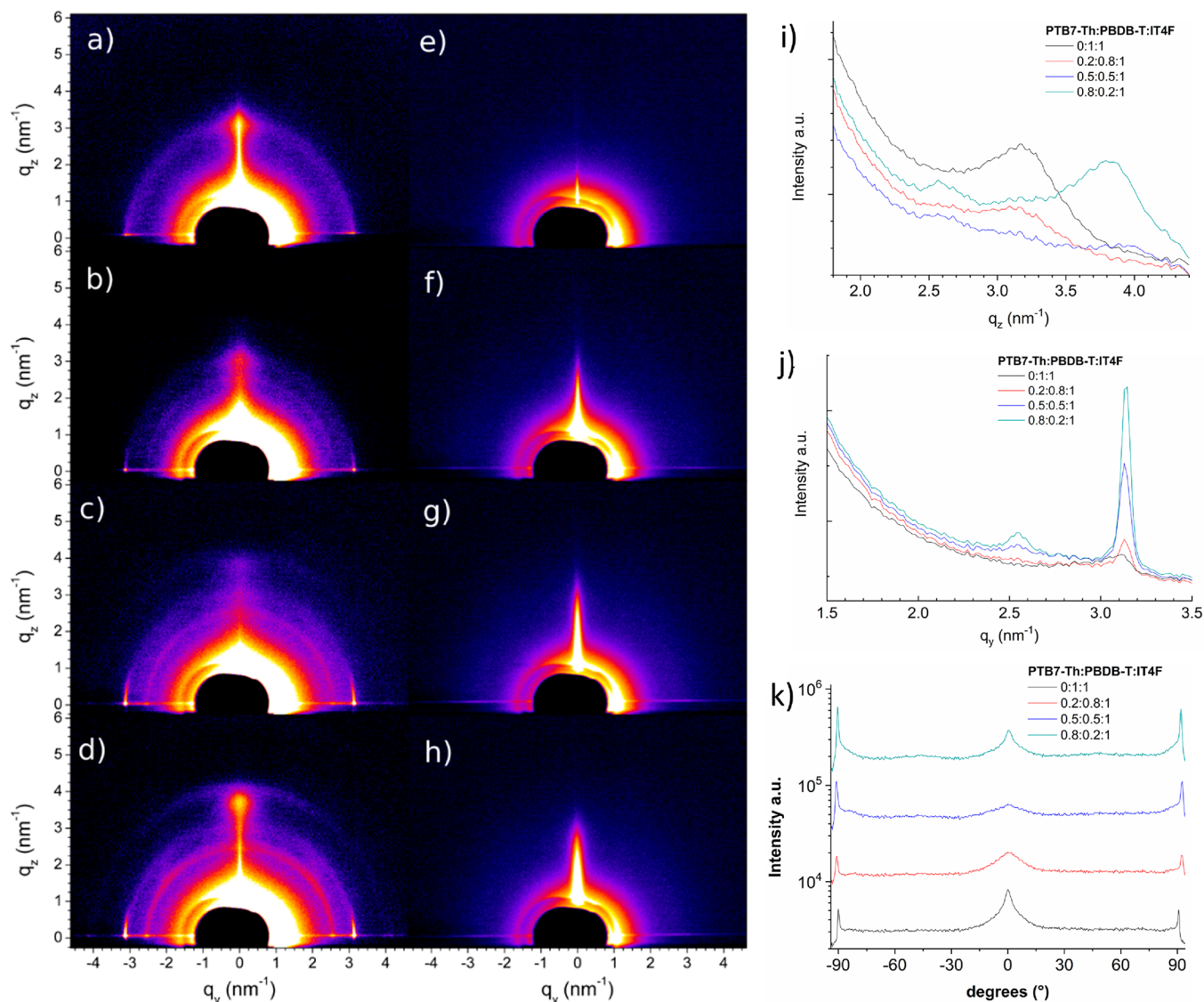


Figure 6. GIXD data of PTB7-Th:PBDB-T:IT4F in mixing ratios (a) 0:1:1, (b) 0.2:0.8:1, (c) 0.5:0.5:1, and (d) 0.8:0.2:1 and data from PTB7-Th:PCDTBT:IT4F in mixing ratios (e) 0:1:1, (f) 0.5:0.5:1, (g) 0.95:0.05:1, and (h) 1:0:1. Cuts through the GIXD data of PTB7-Th:PBDB-T:IT4F shown in the left panel in different mixing ratios. (i) Integration along the out-of-plane direction (q_z) neglecting data with nonzero in-plane component. (j) Integration along the in-plane direction (q_y) at $q_z = 0$. (k) Radial intensity profile at $q = 3.15 \text{ nm}^{-1}$ with 0° corresponding to $q_y = 0$.

which is also clear from the integration along the q_z -axis (Figure 6i). In addition, we attribute the reflection at $q_z = 3.14 \text{ nm}^{-1}$ to phase separating pure PTB7-Th domains.⁵⁹ Therefore, we conclude that the PBDB-T and PTB7-Th do not form a mixed stacking but exist in separate domains, as inferred from device characteristics and AFM images discussed previously. From the radial profiles at $q_z = 3.14 \text{ nm}^{-1}$ (Figure 6j) we observe that the mosaicity (orientational domain distribution) is largest for intermediate mixing ratios 1:0.5:0.5 in the ternary blend. In addition, we find the reflection corresponding to the in-plane stacking ($q_y = 3.14 \text{ nm}^{-1}$), which is relatively weak and broad in the binary PBDB-T:IT4F mixture to sharpen and intensify upon addition of PTB7-Th (Figure 6k). From this observation, we conclude that the in-plane stacking quality for high ratios of PTB7-Th in the ternary blend is strongly improved, and hence for the higher ratio of PTB7-Th, we observed optimal device performances.

In comparison to ternary blends of PTB7-Th:PBDB-T:IT4F, which show relatively strong crystalline order, we find only

very weak ordering in PTB7-Th:PCDTBT:IT4F mixtures (Figure 6e–h). Instead of clear Bragg reflections, we find here a diffuse halo in the range of $q = 2.0\text{--}3.0 \text{ nm}^{-1}$ without a preferred distribution. This feature is consistent with phase-separated pure PTB7-Th.⁵⁹ Its intensity increased for lower PCDTBT content, and because no Bragg reflection from PCDTBT is observed, we conclude that the PCDTBT is not structurally well ordered. The observation of a similar diffraction pattern from PTB7-Th:IT4F (Figure 6h) and the optimized blend PTB7-Th:PCDTBT:IT4F (0.95:0.05:1) (Figure 6g) suggests that the inclusion of 5 wt % PCDTBT in PTB7-Th:IT4F did not disrupt the packing but rather helped in charge extraction, thereby increasing the photocurrent. We find a slightly different shape of the reflectivity ridge along q_z ($q_y = 0$), which is likely based on the different morphology and surface properties of the blend.

Finally, to understand the surface properties of the blends, we performed contact angle measurements of water and diiodomethane droplets on the pristine films of all the

components (Figure S10). From the measured contact angles, by using the Owens method,⁶⁰ we determined surface energies of the respective films. The interfacial surface energies were then calculated following Neumann's method.⁶¹ Table S7 depicts the contact angles and calculated surface energy values of the four materials. The wetting coefficients (ω) of PCDTBT, PBDB-T, and PTB7-Th were then calculated by using Young's equation.⁶² From the values of ω , it was found that PCDTBT indeed lies at the interface of PTB7-Th and IT4F, thereby facilitating the charge and energy transfer. This is in line with the results observed from AFM and GIXD studies, and in the cases of PBDB-T and PTB7-Th, the wetting coefficient values suggested that they both are dispersed in IT4F domains, thereby promoting the FRET between the two as supported by the TAS and device data discussed earlier. The details of calculation are shown in the Supporting Information.

3. CONCLUSION

We have probed the role of FRET and blend morphology in enhancing the PCE of two TBSCs containing polymer donors: PCDTBT and PBDB-T. Our study shows that blend morphology is playing a prominent role in enhancing the device photocurrent in PBDB-T-based TBSC by reducing the carrier recombination loss without compromising the exciton generation. But in the case of PCDTBT-based TBSC, because of morphological incompatibility of PCDTBT with IT4F, a lower loading percentage of PCDTBT yielded optimum performance. Because of this, FRET could not be manifested to its full extent although the spectroscopic evidence independently confirmed higher FRET efficiency between PTB7-Th and PCDTBT with higher loading percentage of PCDTBT. The device performances were analyzed to understand the origin of V_{OC} , exciton generation, charge transfer, and charge collection probabilities in optimized binary and ternary blends. All the blends except PCDTBT:IT4F showed efficient and near unity charge generation and collection. Upon incorporation of PCDTBT or PBDB-T in the PTB7-Th:IT4F blend, the enhanced D/A interface suppressed geminate recombination, hence improving exciton dissociation and charge extraction in the resulting TBSCs. This effect was very prominent in the case of PBDB-T and resulted in highest PCE. The improved exciton generation rate in the case of PCDTBT-based TBSC as compared to its binary counterpart is a direct consequence of FRET between the polymer donors and improved morphology. For PBDB-T-based TBSC, it is cumulative effect of reduced carrier recombination, increased carrier mobility, and improved blend morphology which helped realize the highest device efficiency. Insights from PDS, $J-V$ data, and contact angle measurements confirmed that PCDTBT is lying at the interface of PTB7-Th and IT4F, thereby facilitating charge transfer between the three; however, PBDB-T could be forming parallel-like arrangement in the blend to achieve effective charge and energy transfer. This was well corroborated from GIXD analysis and AFM studies. We conclude that the blend morphology plays a dominant role in dictating the photophysical processes such as FRET, and hence the resulting device performance is limited by thin film morphology of the ternary blend.

■ ASSOCIATED CONTENT

Supporting Information

The Supporting Information is available free of charge at <https://pubs.acs.org/doi/10.1021/acsaem.0c02179>.

Materials and methods, FRET distance calculation, TA spectra of pristine polymer films, 3D TA contour maps of neat and blend films, tables containing SCLC mobility values, controlled device parameters with varying composition, exciton dissociation probabilities, diode ideality factors, intensity-dependent $J-V$ characteristics, PDS of neat and blend films with E_{CT} analysis, AFM images of control binary and ternary blends, contact angles and surface energy calculation (PDF)

■ AUTHOR INFORMATION

Corresponding Authors

Satish Patil – Solid State and Structural Chemistry Unit, Indian Institute of Science, Bangalore 560012, India; orcid.org/0000-0003-3884-114X; Email: spatil@iisc.ac.in

Richard H. Friend – Cavendish Laboratory, University of Cambridge, Cambridge CB3 0HE, United Kingdom; orcid.org/0000-0001-6565-6308; Email: rhf10@cam.ac.uk

Authors

Aiswarya Abhisek Mohapatra – Solid State and Structural Chemistry Unit, Indian Institute of Science, Bangalore 560012, India; orcid.org/0000-0002-4633-7771

Ravichandran Shivanna – Cavendish Laboratory, University of Cambridge, Cambridge CB3 0HE, United Kingdom; orcid.org/0000-0002-0915-6066

Suresh Podapangi – Solid State and Structural Chemistry Unit, Indian Institute of Science, Bangalore 560012, India

Alexander Hinderhofer – Institut für Angewandte Physik, Universität Tübingen, Tübingen 72076, Germany; orcid.org/0000-0001-8152-6386

M. Ibrahim Dar – Cavendish Laboratory, University of Cambridge, Cambridge CB3 0HE, United Kingdom; orcid.org/0000-0001-9489-8365

Nilabja Maity – Solid State and Structural Chemistry Unit, Indian Institute of Science, Bangalore 560012, India

Frank Schreiber – Institut für Angewandte Physik, Universität Tübingen, Tübingen 72076, Germany

Aditya Sadhanala – Cavendish Laboratory, University of Cambridge, Cambridge CB3 0HE, United Kingdom; Centre for Nano Science and Engineering, Indian Institute of Science, Bangalore 560012, India; orcid.org/0000-0003-2832-4894

Complete contact information is available at: <https://pubs.acs.org/doi/10.1021/acsaem.0c02179>

Notes

The authors declare no competing financial interest.

■ ACKNOWLEDGMENTS

A.A.M., R.S., A.S., M.I.D., S.P., and R.H.F. acknowledge support from the EPSRC project Strategic University Network to Revolutionize Indian Solar Energy-SUNRISE (EP/P032591/1). A.A.M. also acknowledges IISc, Bangalore, for senior research fellowship. R.S. acknowledges the Royal Society Newton International Fellowship. S.P. acknowledges

the Department of Science and Technology, New Delhi, for the Swarnajayanti Fellowship. A.H. and F.S. acknowledge DESY (Hamburg, Germany) for the provision of experimental facilities at PETRA III and thank Florian Bertram for assistance in using beamline P08. M.I.D. acknowledges the financial support from the Swiss National Science Foundation under Project P300P2_174471.

REFERENCES

- (1) Mazzi, K. A.; Luscombe, C. K. The Future of Organic Photovoltaics. *Chem. Soc. Rev.* **2015**, *44* (1), 78–90.
- (2) Kang, H.; Kim, G.; Kim, J.; Kwon, S.; Kim, H.; Lee, K. Bulk-Heterojunction Organic Solar Cells: Five Core Technologies for Their Commercialization. *Adv. Mater.* **2016**, *28*, 7821–7861.
- (3) Brabec, C. J. Organic Photovoltaics: Technology and Market. *Sol. Energy Mater. Sol. Cells* **2004**, *83* (2–3), 273–292.
- (4) Liang, Y.; Xu, Z.; Xia, J.; Tsai, S.-T.; Wu, Y.; Li, G.; Ray, C.; Yu, L. For the Bright Future-Bulk Heterojunction Polymer Solar Cells with Power Conversion Efficiency of 7.4%. *Adv. Mater.* **2010**, *22* (20), E135–E138.
- (5) Zhou, Z.; Liu, W.; Zhou, G.; Zhang, M.; Qian, D.; Zhang, J.; Chen, S.; Xu, S.; Yang, C.; Gao, F.; Zhu, H.; Liu, F.; Zhu, X. Subtle Molecular Tailoring Induces Significant Morphology Optimization Enabling over 16% Efficiency Organic Solar Cells with Efficient Charge Generation. *Adv. Mater.* **2020**, *32*, 1906324.
- (6) Cui, Y.; Yao, H.; Zhang, J.; Zhang, T.; Wang, Y.; Hong, L.; Xian, K.; Xu, B.; Zhang, S.; Peng, J.; Wei, Z.; Gao, F.; Hou, J. Over 16% Efficiency Organic Photovoltaic Cells Enabled by a Chlorinated Acceptor with Increased Open-Circuit Voltages. *Nat. Commun.* **2019**, DOI: 10.1038/s41467-019-10351-5.
- (7) Lin, Y.; Adilbekova, B.; Firdaus, Y.; Yengel, E.; Faber, H.; Sajjad, M.; Zheng, X.; Yari, E.; Seitkhan, A.; Bakr, O. M.; El-Labban, A.; Schwingenschlög, U.; Tung, V.; McCulloch, I.; Laquai, F.; Anthopoulos, T. D. 17% Efficient Organic Solar Cells Based on Liquid Exfoliated WS₂ as a Replacement for PEDOT:PSS. *Adv. Mater.* **2019**, *31* (46), 1902965.
- (8) Yuan, J.; Zhang, Y.; Zhou, L.; Zhang, G.; Yip, H. L.; Lau, T. K.; Lu, X.; Zhu, C.; Peng, H.; Johnson, P. A.; Leclerc, M.; Cao, Y.; Ulanski, J.; Li, Y.; Zou, Y. Single-Junction Organic Solar Cell with over 15% Efficiency Using Fused-Ring Acceptor with Electron-Deficient Core. *Joule* **2019**, *3* (4), 1140–1151.
- (9) Meng, L.; Zhang, Y.; Wan, X.; Li, C.; Zhang, X.; Wang, Y.; Ke, X.; Xiao, Z.; Ding, L.; Xia, R.; Yip, H. L.; Cao, Y.; Chen, Y. Organic and Solution-Processed Tandem Solar Cells with 17.3% Efficiency. *Science (Washington, DC, U. S.)* **2018**, *361* (6407), 1094–1098.
- (10) Rajaram, S.; Shivanna, R.; Kandappa, S. K.; Narayan, K. S. Nonplanar Perylene Diimides as Potential Alternatives to Fullerenes in Organic Solar Cells. *J. Phys. Chem. Lett.* **2012**, *3* (17), 2405–2408.
- (11) Zhao, W.; Qian, D.; Zhang, S.; Li, S.; Inganäs, O.; Gao, F.; Hou, J. Fullerene-Free Polymer Solar Cells with over 11% Efficiency and Excellent Thermal Stability. *Adv. Mater.* **2016**, *28* (23), 4734–4739.
- (12) Zhao, W.; Li, S.; Yao, H.; Zhang, S.; Zhang, Y.; Yang, B.; Hou, J. Molecular Optimization Enables over 13% Efficiency in Organic Solar Cells. *J. Am. Chem. Soc.* **2017**, *139* (21), 7148–7151.
- (13) Song, J.; Li, C.; Zhu, L.; Guo, J.; Xu, J.; Zhang, X.; Weng, K.; Zhang, K.; Min, J.; Hao, X.; Zhang, Y.; Liu, F.; Sun, Y. Ternary Organic Solar Cells with Efficiency > 16.5% Based on Two Compatible Nonfullerene Acceptors. *Adv. Mater.* **2019**, *31*, 1905645.
- (14) Yan, T.; Song, W.; Huang, J.; Peng, R.; Huang, L.; Ge, Z. 16.67% Rigid and 14.06% Flexible Organic Solar Cells Enabled by Ternary Heterojunction Strategy. *Adv. Mater.* **2019**, *31* (39), 1902210.
- (15) Pan, M. A.; Lau, T. K.; Tang, Y.; Wu, Y. C.; Liu, T.; Li, K.; Chen, M. C.; Lu, X.; Ma, W.; Zhan, C. 16.7%-Efficiency Ternary Blended Organic Photovoltaic Cells with PCBM as the Acceptor Additive to Increase the Open-Circuit Voltage and Phase Purity. *J. Mater. Chem. A* **2019**, *7* (36), 20713–20722.
- (16) Fan, B.; Zeng, Z.; Zhong, W.; Ying, L.; Zhang, D.; Li, M.; Peng, F.; Li, N.; Huang, F.; Cao, Y. Optimizing Microstructure Morphology and Reducing Electronic Losses in 1 Cm² Polymer Solar Cells to Achieve Efficiency over 15%. *ACS Energy Lett.* **2019**, *4* (10), 2466–2472.
- (17) Zhou, Z.; Xu, S.; Song, J.; Jin, Y.; Yue, Q.; Qian, Y.; Liu, F.; Zhang, F.; Zhu, X. High-Efficiency Small-Molecule Ternary Solar Cells with a Hierarchical Morphology Enabled by Synergizing Fullerene and Non-Fullerene Acceptors. *Nat. Energy* **2018**, *3* (11), 952–959.
- (18) Liu, S.; Yuan, J.; Deng, W.; Luo, M.; Xie, Y.; Liang, Q.; Zou, Y.; He, Z.; Wu, H.; Cao, Y. High-Efficiency Organic Solar Cells with Low Non-Radiative Recombination Loss and Low Energetic Disorder. *Nat. Photonics* **2020**, *14*, 300.
- (19) Qian, D.; Zheng, Z.; Yao, H.; Tress, W.; Hopper, T. R.; Chen, S.; Li, S.; Liu, J.; Chen, S.; Zhang, J.; Liu, X. K.; Gao, B.; Ouyang, L.; Jin, Y.; Pozina, G.; Buyanova, I. A.; Chen, W. M.; Inganäs, O.; Coropceanu, V.; Bredas, J. L.; Yan, H.; Hou, J.; Zhang, F.; Bakulin, A. A.; Gao, F. Design Rules for Minimizing Voltage Losses in High-Efficiency Organic Solar Cells. *Nat. Mater.* **2018**, *17* (8), 703–709.
- (20) Zhou, R.; Jiang, Z.; Yang, C.; Yu, J.; Feng, J.; Adil, M. A.; Deng, D.; Zou, W.; Zhang, J.; Lu, K.; Ma, W.; Gao, F.; Wei, Z. All-Small-Molecule Organic Solar Cells with over 14% Efficiency by Optimizing Hierarchical Morphologies. *Nat. Commun.* **2019**, *10* (1), 5393.
- (21) Liu, J.; Chen, S.; Qian, D.; Gautam, B.; Yang, G.; Zhao, J.; Bergqvist, J.; Zhang, F.; Ma, W.; Ade, H.; Inganäs, O.; Gundogdu, K.; Gao, F.; Yan, H. Fast Charge Separation in a Non-Fullerene Organic Solar Cell with a Small Driving Force. *Nat. Energy* **2016**, DOI: 10.1038/nenergy.2016.89.
- (22) Hou, J.; Inganäs, O.; Friend, R. H.; Gao, F. Organic Solar Cells Based on Non-Fullerene Acceptors. *Nat. Mater.* **2018**, *17*, 119–128.
- (23) Shockley, W.; Queisser, H. J. Detailed Balance Limit of Efficiency of P-n Junction Solar Cells. *J. Appl. Phys.* **1961**, *32* (3), 510–519.
- (24) Mohapatra, A. A.; Kim, V.; Puttaraju, B.; Sadhanala, A.; Jiao, X.; Mcneill, C. R.; Friend, R. H.; Patil, S. Förster Resonance Energy Transfer Drives Higher Efficiency in Ternary Blend Organic Solar Cells. *ACS Appl. Energy Mater.* **2018**, *1* (9), 4874–4882.
- (25) Liu, J.; Tang, B.; Liang, Q.; Han, Y.; Xie, Z.; Liu, J. Dual Förster Resonance Energy Transfer and Morphology Control to Boost the Power Conversion Efficiency of All-Polymer OPVs. *RSC Adv.* **2017**, *7* (22), 13289–13298.
- (26) Li, W.; Yan, Y.; Gong, Y.; Cai, J.; Cai, F.; Gurney, R. S.; Liu, D.; Pearson, A. J.; Lidzey, D. G.; Wang, T. Contrasting Effects of Energy Transfer in Determining Efficiency Improvements in Ternary Polymer Solar Cells. *Adv. Funct. Mater.* **2018**, *28* (5), 1704212.
- (27) Goh, T.; Huang, J. S.; Bartolome, B.; Sfeir, M. Y.; Vaisman, M.; Lee, M. L.; Taylor, A. D. Panchromatic Polymer-Polymer Ternary Solar Cells Enhanced by Förster Resonance Energy Transfer and Solvent Vapor Annealing. *J. Mater. Chem. A* **2015**, *3* (36), 18611–18621.
- (28) Huang, J. S.; Goh, T.; Li, X.; Sfeir, M. Y.; Bielinski, E. A.; Tomasulo, S.; Lee, M. L.; Hazari, N.; Taylor, A. D. Polymer Bulk Heterojunction Solar Cells Employing Förster Resonance Energy Transfer. *Nat. Photonics* **2013**, *7* (6), 479–485.
- (29) Gasparini, N.; Kahmann, S.; Salvador, M.; Perea, J. D.; Sperlich, A.; Baumann, A.; Li, N.; Rechberger, S.; Spiecker, E.; Dyakonov, V.; Portale, G.; Loi, M. A.; Brabec, C. J.; Ameri, T. Favorable Mixing Thermodynamics in Ternary Polymer Blends for Realizing High Efficiency Plastic Solar Cells. *Adv. Energy Mater.* **2019**, *9* (19), 1803394.
- (30) Gupta, V.; Bharti, V.; Kumar, M.; Chand, S.; Heeger, A. J. Polymer-Polymer Förster Resonance Energy Transfer Significantly Boosts the Power Conversion Efficiency of Bulk-Heterojunction Solar Cells. *Adv. Mater.* **2015**, *27* (30), 4398–4404.
- (31) Scully, S. R.; Armstrong, P. B.; Edder, C.; Fréchet, J. M. J.; McGehee, M. D. Long-Range Resonant Energy Transfer for Enhanced Exciton Harvesting for Organic Solar Cells. *Adv. Mater.* **2007**, *19* (19), 2961–2966.

- (32) Cnops, K.; Rand, B. P.; Cheyns, D.; Verreert, B.; Empl, M. A.; Heremans, P. 8.4% Efficient Fullerene-Free Organic Solar Cells Exploiting Long-Range Exciton Energy Transfer. *Nat. Commun.* **2014**, *5* (1), 1–6.
- (33) Luhman, W. A.; Holmes, R. J. Investigation of Energy Transfer in Organic Photovoltaic Cells and Impact on Exciton Diffusion Length Measurements. *Adv. Funct. Mater.* **2011**, *21* (4), 764–771.
- (34) Liu, C.; Zhang, D.; Lu, F.; Tan, M.; Luan, T.; Wu, H.; Zhang, B.; Shen, L.; Guo, W. Overcoming Defect-Induced Charge Recombination Loss in Organic Solar Cells by Förster Resonance Energy Transfer. *ACS Sustainable Chem. Eng.* **2018**, *6* (8), 9699–9706.
- (35) Weu, A.; Kumar, R.; Butscher, J. F.; Lami, V.; Paulus, F.; Bakulin, A. A.; Yaynzof, Y. Energy Transfer to a Stable Donor Suppresses Degradation in Organic Solar Cells. *Adv. Funct. Mater.* **2020**, *30*, 1907432.
- (36) Xie, Y.; Li, T.; Guo, J.; Bi, P.; Xue, X.; Ryu, H. S.; Cai, Y.; Min, J.; Huo, L.; Hao, X.; Woo, H. Y.; Zhan, X.; Sun, Y. Ternary Organic Solar Cells with Small Nonradiative Recombination Loss. *ACS Energy Lett.* **2019**, *4* (5), 1196–1203.
- (37) Khlyabich, P. P.; Burkhart, B.; Thompson, B. C. Efficient Ternary Blend Bulk Heterojunction Solar Cells with Tunable Open-Circuit Voltage. *J. Am. Chem. Soc.* **2011**, *133* (37), 14534–14537.
- (38) Street, R. A.; Davies, D.; Khlyabich, P. P.; Burkhart, B.; Thompson, B. C. Origin of the Tunable Open-Circuit Voltage in Ternary Blend Bulk Heterojunction Organic Solar Cells. *J. Am. Chem. Soc.* **2013**, *135* (3), 986–989.
- (39) Gasparini, N.; Salleo, A.; McCulloch, I.; Baran, D. The Role of the Third Component in Ternary Organic Solar Cells. *Nat. Rev. Mater.* **2019**, *4*, 229–242.
- (40) Xu, X.; Bi, Z.; Ma, W.; Wang, Z.; Choy, W. C. H.; Wu, W.; Zhang, G.; Li, Y.; Peng, Q. Highly Efficient Ternary-Blend Polymer Solar Cells Enabled by a Nonfullerene Acceptor and Two Polymer Donors with a Broad Composition Tolerance. *Adv. Mater.* **2017**, *29* (46), 1704271.
- (41) Lee, S. K.; Cho, J. M.; Goo, Y.; Shin, W. S.; Lee, J. C.; Lee, W. H.; Kang, I. N.; Shim, H. K.; Moon, S. J. Synthesis and Characterization of a Thiazolo[5,4-d]Thiazole-Based Copolymer for High Performance Polymer Solar Cells. *Chem. Commun.* **2011**, *47* (6), 1791–1793.
- (42) Qian, D.; Ye, L.; Zhang, M.; Liang, Y.; Li, L.; Huang, Y.; Guo, X.; Zhang, S.; Tan, Z.; Hou, J. Design, Application, and Morphology Study of a New Photovoltaic Polymer with Strong Aggregation in Solution State. *Macromolecules* **2012**, *45* (24), 9611–9617.
- (43) Lin, Y.; Wang, J.; Zhang, Z. G.; Bai, H.; Li, Y.; Zhu, D.; Zhan, X. An Electron Acceptor Challenging Fullerenes for Efficient Polymer Solar Cells. *Adv. Mater.* **2015**, *27* (7), 1170–1174.
- (44) Benten, H.; Nishida, T.; Mori, D.; Xu, H.; Ohkita, H.; Ito, S. High-Performance Ternary Blend All-Polymer Solar Cells with Complementary Absorption Bands from Visible to near-Infrared Wavelengths. *Energy Environ. Sci.* **2016**, *9* (1), 135–140.
- (45) Valeur, B.; Berberan-Santos, M. N. *Molecular Fluorescence*; Wiley-VCH Verlag GmbH & Co. KGaA: Weinheim, Germany, 2012.
- (46) de Mello, J. C.; Wittmann, H. F.; Friend, R. H. An Improved Experimental Determination of External Photoluminescence Quantum Efficiency. *Adv. Mater.* **1997**, *9* (3), 230–232.
- (47) Chen, M.; Liu, D.; Li, W.; Gurney, R. S.; Li, D.; Cai, J.; Spooner, E. L. K.; Kilbride, R. C.; McGettrick, J. D.; Watson, T. M.; Li, Z.; Jones, R. A. L.; Lidzey, D. G.; Wang, T. Influences of Non-Fullerene Acceptor Fluorination on Three-Dimensional Morphology and Photovoltaic Properties of Organic Solar Cells. *ACS Appl. Mater. Interfaces* **2019**, *11* (29), 26194–26203.
- (48) Ma, X.; Mi, Y.; Zhang, F.; An, Q.; Zhang, M.; Hu, Z.; Liu, X.; Zhang, J.; Tang, W. Efficient Ternary Polymer Solar Cells with Two Well-Compatible Donors and One Ultranarrow Bandgap Nonfullerene Acceptor. *Adv. Energy Mater.* **2018**, *8* (11), 1702854.
- (49) Cowan, S. R.; Roy, A.; Heeger, A. J. Recombination in Polymer-Fullerene Bulk Heterojunction Solar Cells. *Phys. Rev. B: Condens. Matter Mater. Phys.* **2010**, DOI: 10.1103/PhysRevB.82.245207.
- (50) Koster, L. J. A.; Mihailetchi, V. D.; Ramaker, R.; Blom, P. W. M. Light Intensity Dependence of Open-Circuit Voltage of Polymer-Fullerene Solar Cells. *Appl. Phys. Lett.* **2005**, *86* (12), 123509.
- (51) Schilinsky, P.; Waldauf, C.; Brabec, C. J. Recombination and Loss Analysis in Polythiophene Based Bulk Heterojunction Photodetectors. *Appl. Phys. Lett.* **2002**, *81* (20), 3885–3887.
- (52) Riedel, I.; Parisi, J.; Dyakonov, V.; Lutsen, L.; Vanderzande, D.; Hummelen, J. C. Effect of Temperature and Illumination on the Electrical Characteristics of Polymer-Fullerene Bulk-Heterojunction Solar Cells. *Adv. Funct. Mater.* **2004**, *14* (1), 38–44.
- (53) Gebeyehu, D.; Pfeiffer, M.; Maennig, B.; Drechsel, J.; Werner, A.; Leo, K. Highly Efficient P-i-n Type Organic Photovoltaic Devices. *Thin Solid Films* **2004**, *451–452*, 29–32.
- (54) Koster, L. J. A.; Mihailetchi, V. D.; Xie, H.; Blom, P. W. M. Origin of the Light Intensity Dependence of the Short-Circuit Current of Polymer/Fullerene Solar Cells. *Appl. Phys. Lett.* **2005**, *87* (20), 203502.
- (55) Rose, A. *Concepts in Photoconductivity and Allied Problems*; Wiley: New York, 1963.
- (56) Cowan, S. R.; Roy, A.; Heeger, A. J. Recombination in Polymer-Fullerene Bulk Heterojunction Solar Cells. *Phys. Rev. B: Condens. Matter Mater. Phys.* **2010**, *82* (24), 245207.
- (57) Lu, L.; Xu, T.; Chen, W.; Landry, E. S.; Yu, L. Ternary Blend Polymer Solar Cells with Enhanced Power Conversion Efficiency. *Nat. Photonics* **2014**, *8* (9), 716–722.
- (58) Zhang, K.-N.; Niu, M.-S.; Jiang, Z.-N.; Chen, Z.-H.; Wang, T.; Wei, M.-M.; Qin, C.-C.; Feng, L.; Qin, W.; So, S.-K.; Hao, X.-T. Multiple Temporal-Scale Photocarrier Dynamics Induced by Synergistic Effects of Fluorination and Chlorination in Highly Efficient Nonfullerene Organic Solar Cells. *Sol. RRL* **2020**, *4* (4), 1900552.
- (59) Wang, W.; Yan, C.; Lau, T. K.; Wang, J.; Liu, K.; Fan, Y.; Lu, X.; Zhan, X. Fused Hexacyclic Nonfullerene Acceptor with Strong Near-Infrared Absorption for Semitransparent Organic Solar Cells with 9.77% Efficiency. *Adv. Mater.* **2017**, *29* (31), 1701308.
- (60) Owens, D. K.; Wendt, R. C. Estimation of the Surface Free Energy of Polymers. *J. Appl. Polym. Sci.* **1969**, *13* (8), 1741–1747.
- (61) Li, D.; Neumann, A. W. A Reformulation of the Equation of State for Interfacial Tensions. *J. Colloid Interface Sci.* **1990**, *137* (1), 304–307.
- (62) Sumita, M.; Sakata, K.; Asai, S.; Miyasaka, K.; Nakagawa, H. Dispersion of Fillers and the Electrical Conductivity of Polymer Blends Filled with Carbon Black. *Polym. Bull.* **1991**, *25* (2), 265–271.